Self-Association of Disulfide-Dimerized Melittin Analogues†

Jiro Takei, Attila Reményi,‡ Anthony R. Clarke, and Christopher E. Dempsey*

Department of Biochemistry and Molecular Recognition Centre, School of Medical Sciences, University of Bristol, University Walk, Bristol BS8 1TD, U.K.

Received November 26, 1997

ABSTRACT: Two cysteine substitutions of bee venom melittin have been synthesized to investigate the effects of disulfide cross-linking on the self-association properties of the peptide in solution. K23C melittin (mltK23C) was designed to link nonpolar surfaces of the amphipathic melittin helix on the basis of the close juxtaposition of pairs of K23 side chains in the crystal of the native melittin tetramer. K23Q/Q25C melittin (mltQ25C) was designed to link the polar surfaces of the peptide such that self-association in membrane bound states might be stabilized. The mltK23C disulfide dimer, $(mltK23C)_2$, is highly structured at low pH under conditions where native melittin, and the mltK23C monomer, are unstructured. High-resolution NMR, circular dichroism, and fluorescence spectroscopy established that $(mltK23C)_2$ is a helical monomer (pseudodimer) with stable helical segments between residues 2−13 and 15−25. Although the symmetrical nature of the pseudodimer prevented high-resolution structure determination, analysis of calculated hydrogen bond lengths, chemical shifts, near-UV circular dichroism, and urea denaturation demonstrated similarities with α-helical coiled coils and with the structure of native melittin in methanol. Stopped flow fluorescence showed that $(mltK23C)_2$ underwent pH- and divalent anion-linked dimerization to a melittin-like pseudotetramer, indicating that a pair of disulfide bonds could be accommodated in a structure similar to the native melittin crystal structure. Despite incorporation of two disulfide bonds into the melittin tetramer, the folding free energy (ΔG_w) of $[(mltK23C)_2]_2$ was similar to that for the native melittin tetramer under the condition used. Incorporation of a disulfide bond on the polar helix face in melittin did not stabilize helical structure in the absence of self-association. Instead, this molecule underwent pH- and divalent anion-linked self-association to an ill-defined aggregate which precipitated.

Melittin (Figure 1) is a 26-amino acid peptide toxin from the venom of the European honey bee (*Apis mellifera*) which undergoes reversible self-associations that underlie many of its properties in solution and in membranes. In aqueous solution, unstructured melittin monomers are in equilibrium with a tetrameric state composed of α-helical monomers. At low pH, and in the absence of divalent anions, the equilibrium lies well toward the unstructured monomer so that, at concentrations of a few millimolar or less, tetramers cannot be detected spectroscopically. At high pH (above the pK_a of the N-terminal amino group), at high ionic strength, and particularly in the presence of divalent anions, the melittin tetramer predominates. Stable dimers of native melittin have never been identified (*1*).

The toxic properties of melittin result from its interactions with bilayer membranes, which are manifest in several characteristic effects (reviewed in ref *2*). At low concentrations, melittin induces anion-selective, voltage-dependent ion conductance in planar bilayers, a phenomenon thought to result from voltage-dependent recruitment of helical monomers into a transmembrane barrel array composed of four or more monomers surrounding an aqueous lumen through which ions permeate. At higher concentrations, the peptide causes membrane destabilization, resulting in hemolysis or dye leakage in erythrocytes or bilayer vesicles, respectively. In saturated phosphatidylcholine membranes, melittin causes reversible bilayer disk micellization which is modulated by the lipid phase transition (*3*, *4*).

Melittin:	G I G A V_5 L K V L T_{10} T G L P A_{15} L I S W I_{20} K R K R Q_{25} Q–NH_2
mltK23C:	G I G A V_5 L K V L T_{10} T G L P A_{15} L I S W I_{20} K R C R Q_{25} Q–NH_2
mltQ25C:	G I G A V_5 L K V L T_{10} T G L P A_{15} L I S W I_{20} K R Q R C_{25} Q–NH_2

FIGURE 1: Amino acid sequences of melittin and its cysteine analogues.

The solution and membrane properties of melittin can generally be understood in terms of the formation of a positively charged amphipathic helical structure (bent due to the structural perturbations induced by the proline 14 residue; Figure 1), upon interaction with a polar−nonpolar interface. The crystal structure of the aqueous tetramer (*5*) shows a well-packed bundle of helical monomers stabilized by interhelical side chain interactions along the nonpolar helical surfaces and solvated by the positively charged polar helix surfaces. The tetramer−monomer equilibrium is modulated by interactions which alter the high positive charge density so that a decrease in charge density through titration of the N-terminal amino group, or selective binding of divalent anions, strongly stabilizes the tetramer. In

† This work was partly funded by the Wellcome Trust through Equipment Grant 040104/Z/93 and the BBSRC through support of the Bristol Centre for Molecular Recognition.

* Corresponding author. Telephone: (0)117 9287569. Fax: (0)117 9288274. E-mail: C.Dempsey@bristol.ac.uk.

‡ Present address: European Molecular Biology Laboratory, 69126 Heidelberg, Germany.

S0006-2960(97)02900-0 CCC: $15.00
Published on Web 03/28/1998

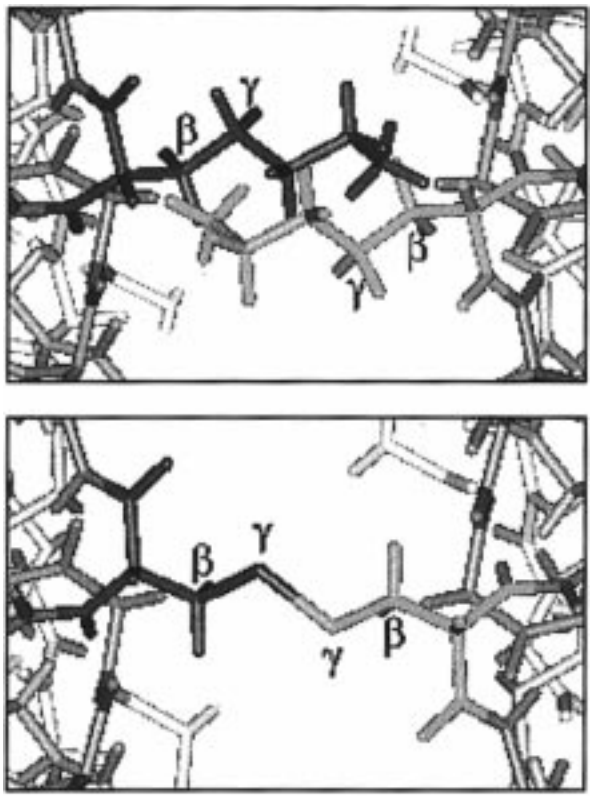

FIGURE 2: Interface between parallel pairs of monomers near the C terminus in the melittin tetramer crystal structure (*5*), illustrating the juxtaposition of pairs of Lys23 side chains (top). The bottom panel illustrates the same region of the melittin crystal structure obtained after replacement of Lys23 with Cys and formation of a disulfide bond, followed by energy minimization. For clarity, only heavy atoms are shown except for Lys23 (top) or Cys23 (bottom).

membranes, the ion channel state is stabilized by high ionic strength which suppresses C-terminal charge repulsion in the parallel helical associates thought to comprise the conducting channel, and by the presence of the P14 residue which allows the C-terminal charged residues to bend away from the channel axis (*6*).

The introduction of cross-links is expected to alter both the solution and membrane properties of melittin. Stabilization of melittin channels (*7*) and other channels (*8*) by assembly on a template has been shown to be effective, and dimerization of alamethicin has been shown to increase channel lifetimes (*9*). Introduction of cross-links in soluble proteins has been shown to alter stabilities and function (*10*, *11*). The simplest means of cross-linking polypeptides is through the introduction of disulfide bonds, and inspection of the X-ray crystal structure of the aqueous melittin tetramer shows that a disulfide cross-link might be accommodated by replacing lysine 23 with cysteine (see Figure 2). Simple models of potential ion channel states (parallel melittin tetramers) indicate that C-terminal cysteine cross-links are potentially accommodated in channel states (unpublished results). In ideal channel states, the cross-link should be on the polar helix surfaces and this is more compatible with the introduction of cysteine at residue 25. To investigate the effects of these disulfide cross-links on the solution and membrane properties of melittin, we have synthesized two cysteine analogues (mltK23C[1] and mltK23Q/Q25C) and prepared cystine dimers by air oxidation. In this paper, we describe the effects of disulfide cross-linking on the solution structures and self-association properties of these peptides. The effects of disulfide cross-links on the membrane properties of melittin are described elsewhere (J. Takei, A. Reményi, and C. E. Dempsey, in preparation).

MATERIALS AND METHODS

Peptide Synthesis. Melittin and its cysteine-containing analogues (Figure 1) were synthesized by Fmoc solid phase synthesis, by G. Bloomberg (Bristol University Molecular Recognition Centre). Crude peptide obtained after cleavage from the resin and removal of protecting groups was purified by HPLC using a Vydac semipreparative C4 reversed phase column (Hesperia, CA). Peptides were eluted using a linear gradient from 20 to 70% acetonitrile in water (0.1% TFA) over 25 min, and the major component in each peptide run was collected and recovered by freeze-drying. Peptide identity and purity were assessed by mass spectroscopy.

The analogues were dimerized by air oxidation in water at pH 8−9 at room temperature in the dark, monitoring the course of the reaction by HPLC. For each peptide, the reaction was complete after 24 h. Dimerization of the mltK23C monomer resulted in one major component which was slightly more strongly retained on the C4 reversed phase HPLC column than monomeric mltK23C. The dimerized peptide was freeze-dried and used without further purification since it was more than 95% pure on the basis of mass spectrometry and two-dimensional (2D) NMR spectroscopy (Figures 4 and 5). Purified peptides were stored at −20 °C before they were used.

Dimerization of purified mltQ25C yielded two components that could be resolved by HPLC, which had identical masses equivalent to the expected mass of the disulfide bridged dimer. Reduction and reoxidation experiments (not shown) established that the minor component is probably a heterodimer composed of one correct peptide and one with a racemized amino acid. The homodimer with the correct chirality was used in all subsequent experiments.

NMR Spectroscopy. All NMR experiments were carried out using the JEOL alpha 500 spectrometer of the Bristol University Molecular Recognition Centre, operating at a proton frequency of 500 MHz. For structural analysis, the cross-linked mltK23C dimer [hereafter $(mltK23C)_2$] was dissolved in 550 μL of H_2O/D_2O (90:10 v/v) at pH 1.7 at a concentration of 1.15 mM (i.e. 2.3 mM in terms of the melittin monomer). One-dimensional (1D) spectra and 2D NOESY (*12*), DQF-COSY (*13*), and HOHAHA (*14*) spectra were recorded at 25, 33, and 40 °C. The isotropic mixing time for NOESY was 200 ms. The spectral width was 6000 Hz, centered on the solvent resonance which was suppressed using a DANTE pulse sequence (*15*). For 2D experiments, typical data sets consist of 2048 f_2 data points and 350 f_1 data points acquiring 64 transient data points per f_1 increment. The f_1 dimension was zero-filled to 2048 points. 2D data sets were processed using Felix version 2.30 (MSI, San

[1] Abbreviations: 1D, one-dimensional; 2D, two-dimensional; CD, circular dichroism; DQF-COSY, double-quantum filtered correlation spectroscopy; DTT, dithiothreitol; HOHAHA, homonuclear Hartmann−Hahn spectroscopy; mltK23C, melittin K23C analogue; $(mltK23C)_2$, disulfide cross-linked mltK23C; mltQ25C, melittin K23C/Q25C analogue; $(mltQ25C)_2$, disulfide cross-linked mltQ25C; NMR, nuclear magnetic resonance; NOE, nuclear Overhauser enhancement; NOESY, 2D NOE spectroscopy.

Diego, CA) on Silicon Graphics workstations. A 70° shifted squared sinebell window function was applied to the FID in both dimensions. Cross-peak assignment was carried out with the sequential assignment method (*16*).

Self-association of the $(mltK23C)_2$ was examined by line broadening in 1D spectra at various pHs or phosphate concentrations. The peptide concentration of all samples was 200 μM (as monomer).

Amide exchange measurements were carried out in D_2O at 20 °C and pH* 1.7, where pH* is the pH directly measured using a hydrogen electrode without correction for the deuterium isotope effect. A series of 1D data were recorded after increasing times after dissolving freeze-dried peptide in D_2O at pH* 1.7, as well as NOESY, DQF-COSY, and HOHAHA to assist in the cross-peak assignment.

Distance restraints were extracted from NOESY spectra of exchanged and nonexchanged samples. The use of partially exchanged data was particularly advantageous for eliminating spectral ambiguities and identifying inter-residue cross-peaks that belong to slowly exchanging amides. No cross-peaks were assigned to interhelical NOEs. NOE cross-peaks were classified into three categories, and inter-proton distance restraints were set as strong (1.8−3.0 Å), medium (1.8−4.0 Å), or weak (1.8−5.0 Å) according to NOE intensities. Hydrogen bond distance restraints were incorporated for slowly exchanging amide hydrogens. Those distances were 1.8−3.5 Å for d_{NH-O} (i, $i + 4$) and 2.3−4.5 Å for d_{N-O} (i, $i + 4$). Hydrogen bond restraints were included only where secondary structure was sufficiently well defined in the initial calculation to allow unambiguous identification of the amide carbonyl hydrogen bonding partners. Dihedral angle restraints were extracted from well-resolved amide peaks in exchanged or nonexchanged 1D spectra. Because of the symmetrical nature of the dimer, no interchain distance information was obtained. Solution structure calculations were performed using simulated annealing within X-PLOR v. 3.1 (*17*) with the SHAKE protocol (*18*). The calculation was carried out using only one set of distance and dihedral angle restraints starting from one polypeptide chain template without its disulfide cross-linked partner, since no NOEs could be assigned unambiguously to interhelical contacts.

Circular Dichroism Spectroscopy. Circular dichroism spectra were recorded on a Jobin-Yvon CD6 spectrophotometer, using 2 or 0.1 mm path length quartz cells. Dithiothreitol (DTT) was added to solutions of nondimerized monomer peptides at equimolar concentrations to prevent disulfide bridge formation. Near-UV CD spectra of the Trp19 indole were recorded between 250 and 310 nm in 1 cm quartz cuvettes. In far-UV CD measurements, three or four spectra sampled at 0.5 nm intervals with an integration time of 1−2 s were averaged, and the baseline was zeroed at 260 nm before plotting without smoothing.

Fluorescence Spectroscopy. Steady state fluorescence spectra were recorded on a Perkin-Elmer LS50B spectrometer to monitor the environmental change of the single tryptophan residue as an intrinsic fluorophore. For the analysis of pH- or dianion-linked self-association of $(mltK23C)_2$, the sample was excited at 290 nm and the emission was recorded between 300 and 400 nm. For urea denaturation experiments, samples in urea at various concentrations were excited at 285 nm and the emission was measured at 360 nm for 30 s. All steady state data were treated as described in the Appendix.

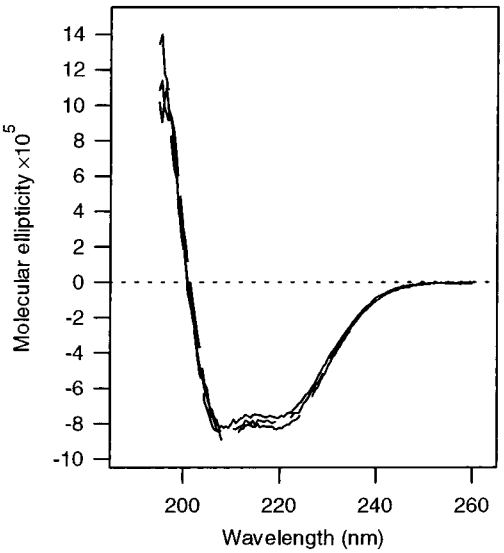

FIGURE 3: Far-UV circular dichroism spectra of $(mltK23C)_2$ in water at pH 1.7, 3.0, and 7.0 from top to bottom at 222 nm. The peptide concentration was 18 μM monomer in each case.

The kinetics of peptide self-association was also studied by stopped flow fluorescence spectroscopy using a sequential stopped flow spectrophotometer (Applied Photophysics). Ninety microliters of 4 or 8 μM peptide solutions at low pH was mixed with an equal volume of the appropriate buffer to generate a jump in pH and/or salt concentration. The sample was excited at 282 nm, and total fluorescence emission above 320 nm was recorded. Transient decays of fluorescence emission in stopped flow experiments were fitted to the standard equation for second-order decay,

$$A_t = A_0/(1 + M_0kt) \quad (1)$$

in which A_t is the amplitude at time t, A_0 is the initial amplitude, M_0 is the peptide concentration, and k is the rate constant for self-association.

RESULTS

$(mltK23C)_2$ Is a Structured Monomer at Low pH. The far-UV CD spectrum of $(mltK23C)_2$ is illustrated in Figure 3 as a function of pH. Unlike native melittin (*19*) and the mltK23C monomer in the presence of DTT (not shown), the peptide is highly helical at low pH. The molecular ellipticity at 222 nm is equivalent to a helical content of around 80%, a value similar to the helical content of the melittin tetramer. The spectrum is essentially independent of pH. For melittin (*19*) and the mltK23C monomer in the presence of DTT, the low-pH state is unstructured and CD ellipticity characteristic of α-helical structure is only observed at high ionic strength.

The downfield regions of the high-resolution NMR spectra containing the nonexchangeable side chain indole resonances of W19 of melittin and $(mltK23C)_2$ at pH* 1.7 and 7.0 in salt-free D_2O, and at pH* 7.0 in the presence of 100 mM sodium phosphate, are shown in Figure 4a. The pH and phosphate effects on the self-association of melittin are well understood. At low pH, the peptide is an unstructured monomer yielding narrow NMR line widths. At pH* 7.0,

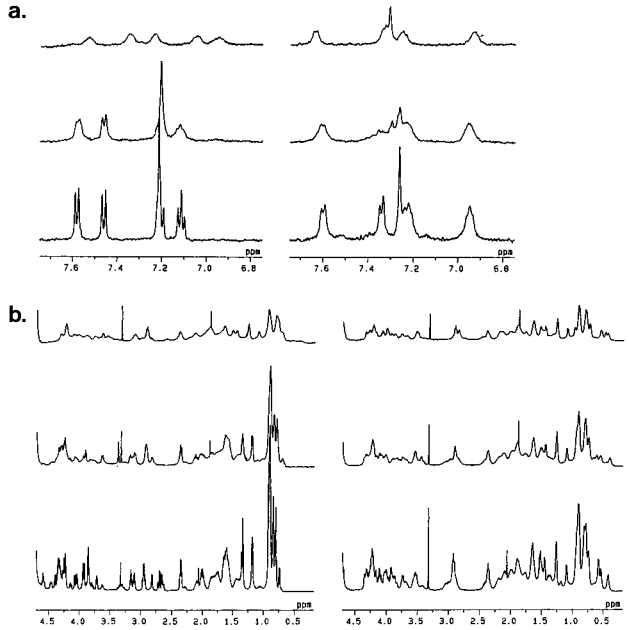

FIGURE 4: (a) Downfield and (b) upfield regions of 1D NMR spectra of melittin (left series) and (mltK23C)$_2$ (right series). In each panel, the solution conditions are as follows: bottom, pH* 1.7 in water; middle, pH* 7.0 in water; and top, pH* 7.0 in 100 mM potassium phosphate.

line broadening is associated with tetramer formation. Under the conditions of the experiment, the monomer predominates, as indicated by the similar chemical shifts of the indole resonances (Figure 4a) and of resonances in the upfield region (Figure 4b) of the spectrum. Only in the presence of phosphate is there a stabilization of the tetrameric state associated with changes in the chemical shifts of the indole resonances and an upfield shift of the envelope of Hα resonances characteristic of helix formation.

At low pH in salt-free solution, the line widths of the NMR signals in the (mltK23C)$_2$ spectrum are intermediate between those of the melittin monomer and tetramer. Consistent with the CD data of Figure 3, the envelope of Hα resonances is shifted upfield, consistent with α-helical structure (see below). At pH* 7.0, the line widths are increased markedly, indicating self-association of the peptide. Neither the increase in pH nor the addition of phosphate has marked effects on the peptide chemical shifts, indicating that the structure in the low-pH state is not greatly affected by self-association.

Solution Structure of (mltK23C)$_2$ at Low pH. Figure 5 shows the HN−HN and Hα−Hβ connectivities in the NOESY spectrum of (mltK23C)$_2$ in water (10% D_2O) at pH 1.7. The 2D NMR spectrum of the peptide was assigned from NOESY, DQF-COSY, and HOHAHA spectra using the sequential assignment method (*16*). A single set of resonances was identified for every residue indicating that the two monomers of the disulfide-linked pair are equivalent. In the amide−amide region (panel a), strong sequential inter-residue connectivities, characteristic of helical structure, were assigned to residues 2−13 (helix I) and 15−25 (helix II), indicating that the monomers are highly helical, consistent with the CD data of Figure 3. In panel b of Figure 5, some well resolved cross-peaks between Hα and Hβ (i, $i + 3$) are boxed with assignments. These characteristic cross-peak

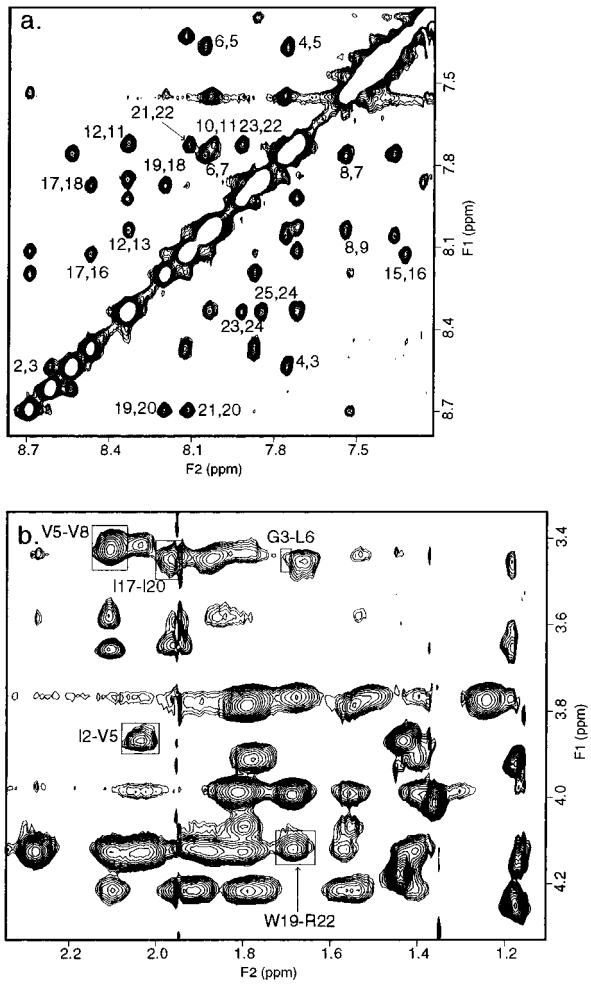

FIGURE 5: Regions of the NOESY spectrum of (mltK23C)$_2$ in water at pH 1.7 at a concentration of 1.15 mM at 25 °C. The mixing time was 200 ms. (a) Amide−amide region showing inter-residue connectivities between adjacent amide hydrogens, annotated with amino acid residue numbers. (b) Hβ (f_2)−Hα (f_1) region. Well-resolved cross-peaks between Hα and Hβ (i, $i + 3$) are boxed with assignments.

patterns confirm the helical conformation of the peptide at low pH.

Solution structures were calculated by imposing distance and dihedral angle constraints onto a monomeric template (not shown). Helices I and II were represented in all low-energy structures. The structure of the connecting region between the two helices was poorly defined with no trend toward a consistent helix bend angle or direction. When two identical sets of restraints were used with a dimer template, the calculations gave no consistent structures and many constraints were violated.

Apparent hydrogen bond lengths for helical amide hydrogens in (mltK23C)$_2$ were calculated using the equation of Wagner et al. (*20*)

$$\Delta\delta = \delta_{HN} - \delta_{random} = 19.2d^{-3} - 2.3 \qquad (2)$$

where δ_{HN} and δ_{random} are the measured and random coil (*16*, *21*) amide chemical shifts, respectively, and d is the hydrogen bond distance (HN−carbonyl O). The calculated hydrogen bond distances are plotted in Figure 6 as a function of the amino acid sequence. Although the chemical shifts may have additional contributions from electrostatic effects and ring

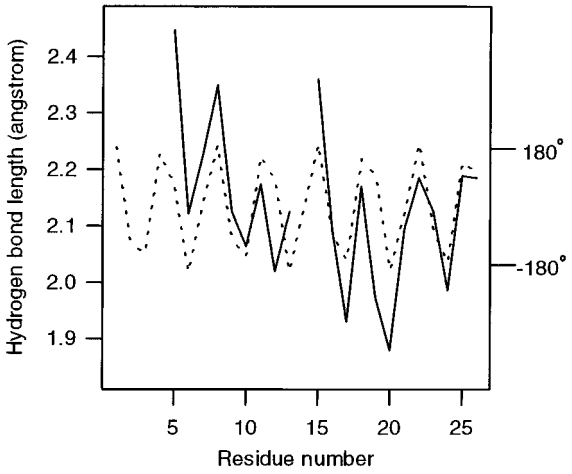

FIGURE 6: Apparent (helical) hydrogen bond lengths for (mltK23C)$_2$ calculated using eq 2 (*20*) (solid line). The dotted line is a sine function defining the radial distribution of amino acid residues around the axis of a regular α-helix.

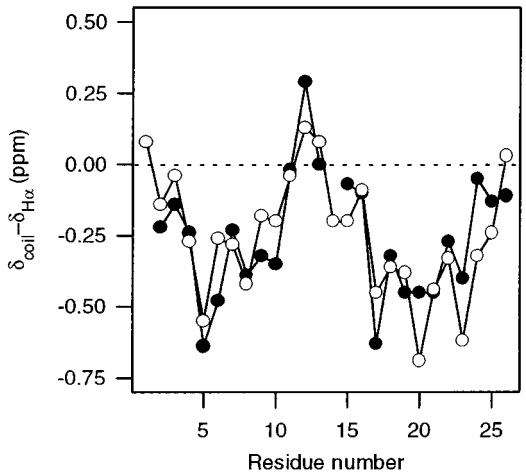

FIGURE 7: Chemical shift deviation from random coil values for CHα atoms of (mltK23C)$_2$ in water at pH 1.7 (●) and melittin in methanol (○). The melittin data are from Bazzo et al. (*22*).

current shifts, they show a marked periodicity with a repeat close to that expected for an α-helix. The short hydrogen bonds lie along the nonpolar helix face, indicating curvature of the helical segments as found in coiled-coil structures. This periodicity results from folding within the (mltK23C)$_2$ pseudodimer since the amide chemical shifts in monomeric (α-helical) melittin in methanol have low periodicity (*22*).

Differences from random coil chemical shift for Hα resonances are plotted for (mltK23C)$_2$ (Figure 7). Data for monomeric (α-helical) melittin in methanol (*22*) are also plotted for comparison. Melittin and (mltK23C)$_2$ show an upfield shift of Hα atoms in the N- and C-terminal helices, with a break of a few downfield-shifted residues near G12. The upfield shift of Hα resonances is further evidence of α-helical structure in the (mltK23C)$_2$ monomer at low pH. The helices are made discontinuous by the presence of P14 which disrupts helical hydrogen bonding near the center of the mltK23C helix in a manner apparently similar to that described for the melittin helix (*22*, *23*).

(mltK23C)$_2$ Undergoes a pH- and Divalent Anion-Linked Dimerization to a Melittin-like Pseudotetramer. The near-UV CD spectra of (mltK23C)$_2$ and melittin are shown in Figure 8. Ellipticity in the absorption bands of the W19 side

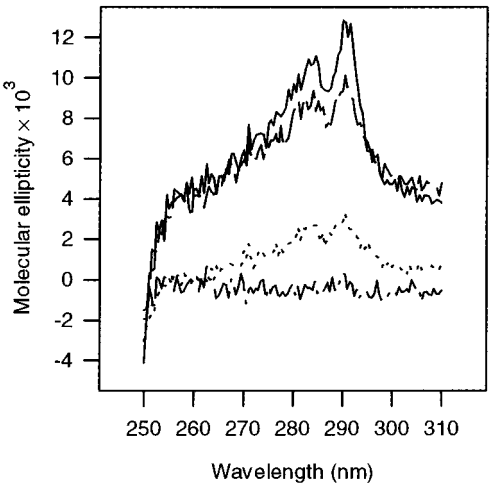

FIGURE 8: Near-UV CD spectra of (mltK23C)$_2$ in water at pH 1.7 (solid line) and at pH 7.5 in 50 mM phosphate (dashed line), melittin in 500 mM phosphate buffer at pH 7.5 (dotted line), and the mltK23C monomer (5 mM DTT) in 500 mM phosphate at pH 7.5 (dotted and dashed line). The peptide concentration was 100 μM for (mltK23C)$_2$ and 200 μM for monomeric mltK23C and melittin.

chain indole indicates that the side chain is constrained within a packed structure (*24*). The spectrum of ellipticities from W19 in (mltK23C)$_2$ is similar to that observed for the melittin tetramer, although the intensities are increased by around 4-fold in the former case, probably as a result of constrained dynamics of the indole side chain since W19 is located on the helix−helix interface directly adjacent to the disulfide at residue 23.

Despite the relative pH independence of the far-UV CD spectrum of (mltK23C)$_2$ and the evidence for well-defined packing of the W19 side chain in the low-pH state, the W19 fluorescence emission spectrum is highly dependent on the pH and the presence of divalent anions (Figure 9). At low pH in the absence of divalent anions [conditions where (mltK23C)$_2$ is a structured monomer], the fluorescence emission spectrum has a maximum near 365 nm. Increasing pH leads to a strong fluorescence quenching and a marked blue shift with a maximum near 338 nm. These properties are very similar to pH- and divalent anion-induced shifts of the native melittin equilibrium from the unstructured monomer to helical tetramer (*25*); in each case, the blue shift and fluorescence quenching are associated with transfer of the W19 indole from a highly solvated state to a nonpolar environment in which the indole is sequestered from interaction with water. Like those with native melittin, the pH- and divalent-anion effects on (mltK23C)$_2$ are associated with self-association as shown by the increased line widths in the ^{1}H NMR spectra of Figure 4 and the transient kinetics described in the following paragraph. The apparent pK_a for self-association of (mltK23C)$_2$ is highly dependent on the buffer composition (Table 1) with highly suppressed apparent pK_as and non-first-order fits to the Henderson−Hasselbalch equation when pH titrations were carried out in dianionic buffers. The titration data obtained in bis-tris (zero dianion concentration) were fitted to a simple equation (eq 8 in Scheme 1 in the Appendix) describing amino deprotonation-linked dimerization, yielding a pK_a (probably the N-terminal amino group) of pH 8.2 under these conditions (Figure 9b and Table 1), which is similar to the values for melittin α-amino titration tabulated in a previous study (*26*).

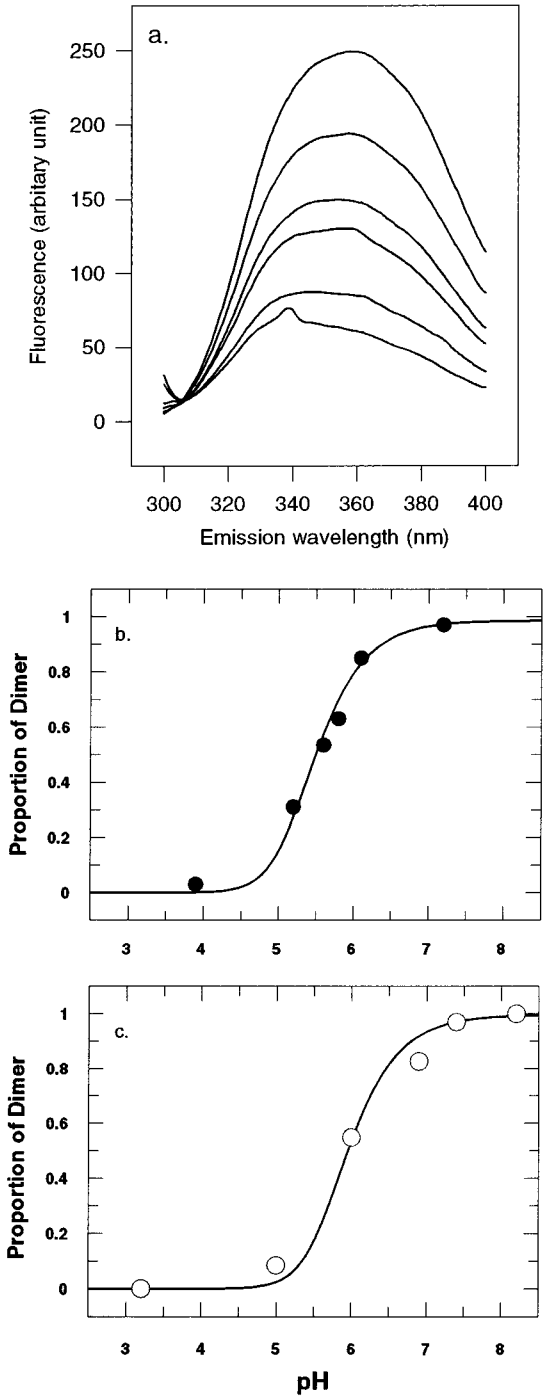

FIGURE 9: (a) Fluorescence spectra of 2 μM (mltK23C)$_2$ in 2 mM phosphate buffer at pH 3.8, 5.2, 5.6, 5.8, 6.1, and 7.4 (top to bottom). The sample was excited at 290 nm, and the slit width was 5 nm. (b) The titration data from panel a were treated according to a dianion-binding model for self-association (Scheme 2 in the Appendix), using eq 11 to determine the proportion of dimerized peptide. The solid line is a fit to eq 13, with fitted parameters listed in Table 1. (c) pH titration for 2 μM (mltK23C)$_2$ in 5 mM bis-tris buffer from fluorescence data similar to that shown in panel a. The data were analyzed using a model for pH-induced self-association (Scheme 1 in the Appendix) from which the proportion of dimer from eq 6 was fitted to eq 8 (solid line), with fitted parameters listed in Table 1.

In dianionic buffers, the titration data were fit to eq 13 describing peptide self-association resulting from multiple binding of dianions (Scheme 2 in the Appendix) in which the association can occur under conditions where the N-terminal amino group remains protonated and the apparent

Table 1: Fitted Parameters for pH- and Ligand-Induced Self-Association of (mltK23C)$_2$

buffer	titration midpoint[a]	pK_a (NH_2)[b]	pK_a (buffer)[c]	n[d]	K
5 mM bis-tris	6.0	8.2			6.0×10^{-11} [e]
2 mM phosphate	5.5		7.2	2	3.0×10^{-15} [f]
10 mM succinate	4.0		5.6	2	8.3×10^{-14} [f]

[a] pH at which the change in fluorescence intensity is half-maximal (see Figure 9). [b] Intrinsic pK_a of the N-terminal amino group (in bis-tris) obtained by fitting data to eq 8 (see the Appendix), with the appropriate constant. See footnote e. [c] Buffer pK_a used to determine [L] (eq 14) for fitting fluorescence emission intensities to eq 13 (see the Appendix). [d] Dianion stoichiometry per pseudotetramer obtained by fitting to eq 13 (see the Appendix). [e] Dissociation constant used in eq 8 (see the Appendix). The constant was independently determined by measuring the guanidinium HCl-induced dissociation of dimer to monomer, under these conditions, incorporating a separate determination of the equilibrium constant for denaturant-induced unfolding of the (mltK23C)$_2$ monomer. [f] Global equilibrium constant in place of $K_L K_D / 2P_O$ in eq 13 (see the Appendix).

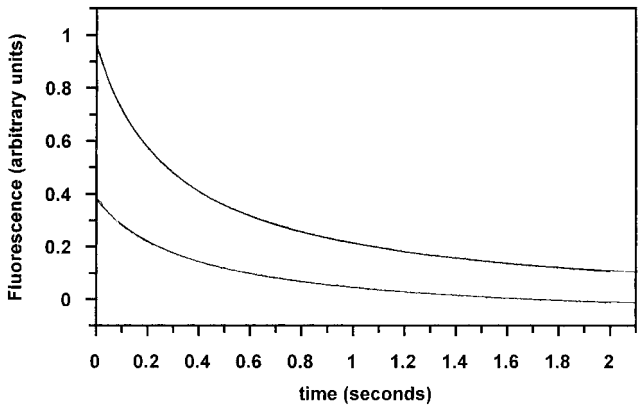

FIGURE 10: Time-resolved fluorescence decay of (mltK23C)$_2$ obtained after a pH and phosphate jump to self-association conditions (e.g. Figure 9a). The total fluorescence emission above 320 nm after mixing 90 μL of peptide in water at pH 3.7 and 90 μL of 100 mM potassium phosphate buffer at pH 7.0 is shown between 0 and 2 s. Postmix peptide concentrations were 2 μM (top) or 4 μM (bottom). The fits of the data using eq 1 are closely superimposed on the experimental fluorescence decay.

pK_as relate to titration of the buffer from monoanionic to dianionic forms (Figure 9c and Table 1).

The molecularity of the rate-limiting step in the pH- and divalent anion-linked self-association resulting in sequestering of the W19 indole was investigated by stopped flow fluorescence spectroscopy. Figure 10 illustrates the time dependence of fluorescence quenching resulting from self-association of (mltK23C)$_2$ after a pH and divalent anion concentration jump (pH 3.7 with a salt-free solution to pH 7.0 with 50 mM sodium phosphate), at postmix concentrations of 2 and 4 μM. The fluorescence decays were fitted to eq 1, yielding values of 2.5×10^6 and 1.6×10^6 mol^{-1} s^{-1} for 2 and 4 μM, respectively, for the second-order association rate constants.

Contribution of Disulfide Linking to Structural Stabilization in (mltK23C)$_2$ and Its Noncovalent Dimer. The equilibrium unfoldings of melittin and the (mltK23C)$_2$ noncovalent dimer were followed by the recovery of fluorescence intensity at 363 nm (see Figure 9) with increasing urea concentration at pH 7.5 in 250 mM sodium phosphate buffer (Figure 11). Data from the linear portions of the curves were

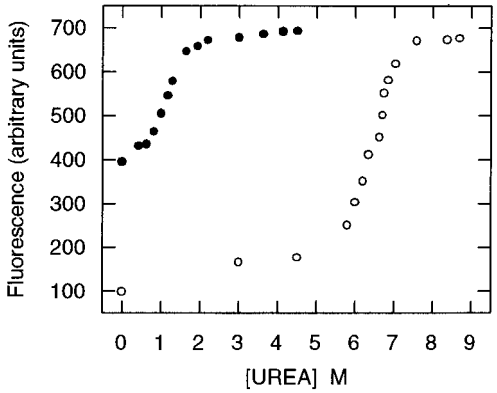

FIGURE 11: Urea-induced increase in fluorescence of $(mltK23C)_2$ (○) and melittin (●) measured at 360 nm, resulting from peptide dissociation and unfolding (e.g. see Figure 9a). The linear part of the data was used to determine ΔG_w (the extrapolated folding free energy at 0 M urea) and m (the number of hydrophobic residues exposed during denaturation) (see Table 2 and the Appendix).

Table 2: Structural Free Energies for Self-Associated Melittin and $(mltK23C)_2$[a]

	ΔG_w (kcal mol^{-1})	m
melittin	−25.0	56.2
$(mltK23C)_2$	−27.1	52.4

[a] Data are from fits to eq 18 (see the Appendix) for the melittin tetramer and the $(mltK23C)_2$ dimer (pseudotetramer) in 250 mM sodium phosphate buffer at pH 7.5.

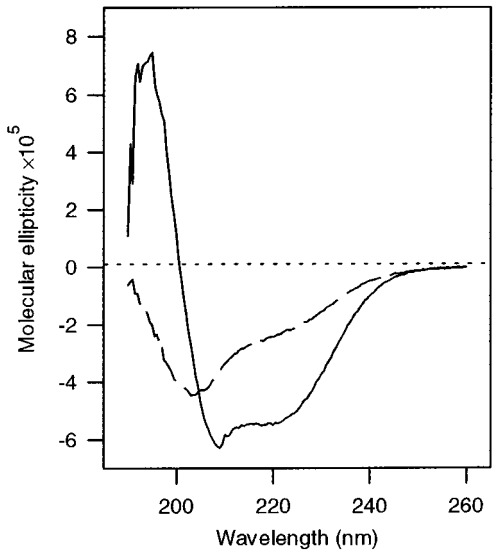

FIGURE 12: Far-UV CD spectra of 18 μM $(mltQ25C)_2$ in phosphate buffer at pH 7.4 (solid line) and in water at pH 2.5 (broken line).

used to determine structural free energies (ΔG_w) and m values for unfolding in denaturant-free solution under these conditions by extrapolation to a urea concentration of zero (see the Appendix). Similar values were obtained for each peptide (Table 2).

Disulfide Positioning on the Polar Helix Face and Its Effects on Structure and Self-Association [(mltQ25C)$_2$]. Unlike $(mltK23C)_2$, $(mltQ25C)_2$ has no stable structure at low pH. Like native melittin, the peptide undergoes a pH- and phosphate-induced shift to a helical conformation as determined by CD (Figure 12). However, at high pH or phosphate concentrations, NMR line widths were very broad (not shown), suggesting the presence of large aggregates. Increasing the peptide concentration to a few millimolar resulted in precipitation.

DISCUSSION

Introduction of a disulfide bond on the hydrophobic interface of two melittin monomers promotes the formation of secondary structure and tertiary interactions in $(mltK23C)_2$, which are stable under conditions where native melittin is unstructured (low peptide concentration, low pH, and absence of divalent anions). Like melittin, in which helix formation in water is linked to the association of amphipathic helices, the stabilization of secondary structure in $(mltK23C)_2$ results from the juxtaposition of melittin monomers that allows packing along a hydrophobic interface. However, stable helical structure cannot be produced by inserting a disulfide bond at random into the melittin sequence as indicated by $(mltQ25C)_2$, which does not have a defined structure in a low-pH, salt-free solution. When the melittin sequence is aligned with the heptad repeat structure of sequences forming amphipathic coiled-coil structures, the disulfide bond falls on position *d* of the helix heptad in mltK23C, which is the optimal position for coiled-coil stabilization by cross-linking (*27*). These authors found from kinetic and modeling studies that disulfide bonds at position *d* are favored over those at position *a* by fulfilling optimal geometrical criteria. Although it might be predicted that relatively minor unfolding of the extreme C terminus of $(mltQ25C)_2$ involving loss of residues 25 and 26 from helical structure would allow packing along the hydrophobic interface within a disulfide-linked structure, this does not occur. Instead, the molecule undergoes pH-, ionic strength-, and concentration-dependent self-association similar to that of native melittin. In $(mltQ25C)_2$, however, the orientation of amphipathic helices is apparently fixed by the intermolecular disulfide bond so that the nonpolar surfaces are directed away from the intramolecular interface, resulting in nonspecific intermolecular association with other $(mltK25Q)_2$ dimers leading to aggregation and precipitation.

Heterogeneity, either structural or through monomer-specific labeling, is required for structure determination of small homodimeric proteins by NMR. O'Donoghue et al. (*28*) showed, by examination of all possible NOEs of homodimeric coiled coils involving HN, Hα, and Hβ atoms, that it is not otherwise possible to distinguish inter- and intrachain NOEs, although these NOEs are most likely to originate from intrachain interactions. By treating all NOEs obtained from $(mltK23C)_2$ involving HN, Hα, and Hβ atoms as intrahelical NOEs, we calculated structures for the mltK23C monomer (not shown) which show similarities and differences compared with the structures of melittin in methanol (*22*) and with α-helical coiled coils. Like melittin, the peptide has two stable α-helical sections encompassing residues 2−13 and 15−25. The Hα chemical shifts are similar for melittin and $(mltK23C)_2$, with upfield shifts characteristic of α-helix in the N- and C-terminal sections. In neither case is structure in the connecting sequence containing P14 well-defined. The α-helical periodicity in estimated hydrogen bond lengths calculated from the amide HN chemical shifts (Figure 6) indicates that the $(mltK23C)_2$ helices are curved with long and short hydrogen bonds on the polar and nonpolar helical surfaces, respectively. Although this type of curvature is characteristic of coiled coils,

the fit of the chemical shift periodicity to a sine function of 3.52 residues per turn (compared with 3.6 for an ideal helix) is lower than the periodicity resulting from classical α-helical coiled-coil supercoiling (e.g. 3.9 residues per turn; *29*), indicating that the $(mltK23C)_2$ molecule does not pack as an ideal coiled coil. Similarly, the structural stabilization of $(mltK23C)_2$ relative to the urea-denatured state of around 2 kcal mol^{-1} (data not shown) is lower than the values found in classical coiled coils.

Since stable melittin (or mltK23C) noncovalent dimers have not been detected spectroscopically at equilibrium, the contribution of disulfide cross-linking to structural stabilization of melittin dimers cannot be determined. Despite the very low stability of noncovalent melittin dimers relative to monomeric or tetrameric states (*1*, *30*), it is likely that the pH- and divalent anion-linked tetramer formation proceeds via a transiently stable dimer (A. Reményi, A. R. Clarke, J. Takei, and C. E. Dempsey, unpublished). Although the structural relationship between $(mltK23C)_2$ and such a folding intermediate is unclear, the peptide is recruited into a melittin-like (pseudo) tetramer under conditions similar to those promoting melittin tetramerization, namely, the binding of dianions and/or an increase in pH for deprotonation of the N-terminal amino group.

Previously, self-association of melittin was analyzed largely in terms of α-amino group titration which reduces charge repulsion between adjacent antiparallel helices in the melittin tetramer (*26*). However, pH titration of $(mltK23C)_2$ shows a pronounced dependence of the apparent pK_a for self-association on the nature of the buffer (Table 1), with pK_a values suppressed well below those expected for α-amino group titration in buffers containing divalent anions. In phosphate and succinate, divalent anions apparently induce self-association under conditions in which the N-terminal amino group remains protonated. In bis-tris, in the absence of divalent anions, self-association is linked to amino group titration. In line with previous measurement of α-amino group titration in melittin (*26*), this is most likely to be the N-terminal α-amino group.

We have derived equations defining the pH-dependent self-association of $(mltK23C)_2$ in the absence (amino group titration, Scheme 1) or presence of divalent anions (dianion-binding model, Scheme 2), as described in the Appendix. From analysis of fluorescence data obtained in pH titration in bis-tris according to Scheme 1, the intrinsic pK_a of the N-terminal amino group of the $(mltK23C)_2$ monomer was found to be 8.20, which is close to the pK_a of 8.15 for melittin in phosphate determined by Zhu et al. (*26*). In bis-tris, the titration midpoint for dimerization is pH 6.0 and self-association is complete at pH values well below the pK_a of the amino group. This results from the strong tendency for self-association of the deprotonated form of $(mltK23C)_2$ ($K_D = 6.0 \times 10^{-11}$), which pulls the equilibrium toward dimerization, and indicates that the amino group pK_a in the associated state under these conditions is suppressed. This is consistent with previous studies which showed that the α-amino group pK_a in the tetrameric state is lower than that of monomeric melittin (*26*).

In phosphate (Figure 9c and Table 1) and succinate (Table 1), self-association of $(mltK23C)_2$ results from the pH-dependent increase in concentration of the dianionic form of the buffer, and the titration data can be fitted to an equation describing dianion binding (Scheme 2 in the Appendix). In succinate, where the apparent pK_a for self-association (titration midpoint, Table 1) is suppressed well below that of the N-terminal amino group, the data could be fitted to eq 18 with the following values: $K_L K_D/2P_O = 8.3 \times 10^{-14}$, $n = 2$, and $pK_{a\ succinate}$ = pH 5.6. The same treatment for the phosphate data yields good fits to the model with the following values: $K_L K_D/2P_O = 3.0 \times 10^{-15}$, $n = 2$, and $pK_{a\ phosphate}$ = pH 7.2. The *n* value, the number of dianions bound per pseudotetramer, can be compared to the number of dianion binding sites in the melittin tetramer. Eisenberg and co-workers located eight bound sulfate ions in the crystal tetramer, four from W19 and K23 of one monomer linking R24 of the neighboring (parallel) monomer and four from R24 to the α-amino group of each antiparallel pair (*31*). The loss of K23 in $(mltK23C)_2$ removes the dianion binding sites linking parallel helices in the pseudotetramer, although this dianion-mediated interaction is replaced by the disulfide cross-link (Figure 2). The retention of dianion sensitivity presumably involves the remaining four dianion binding sites linking antiparallel pairs (R24−G1α). The reduction in dianion stoichiometry determined from the fits of the pH titration data (two dianions per pseudotetramer rather than four) suggests that self-association in solution may not require complete occupation of potential binding sites. The relative affinities of dianions for different binding sites within the melittin tetramer are not known; in the crystal structure, complete occupancy of sites is presumably promoted by the very high concentrations of sulfate used to crystallize the protein.

Despite the introduction of two disulfide cross-links per (pseudo) tetramer in the self-associated $(mltK23C)_2$ dimer, the extrapolated free energy of the folded state relative to the unfolded, dissociated state in water, ΔG_w, and the denaturant sensitivity, *m*, are similar to the values for melittin (Table 2). The similarity in *m*, a measure of the exposure of buried hydrophobic side chains to water upon denaturation (*32*), supports the expectation that the self-associated $(mltK23C)_2$ pseudotetramer has a structure similar to that of the melittin tetramer. The large increase in denaturant concentration required to induce a given degree of dissociation in $(mltK23C)_2$ compared with that needed for melittin under these conditions (Figure 11) is fully accounted for by the conversion of an equilibrium having a fourth-order dependence on peptide concentration to one having a second-order dependence (eq 16 in the Appendix). The absence of disulfide-induced stabilization of the pseudotetramer relative to the melittin tetramer may result from the loss of some dianion-binding stabilizing contributions through the loss of the K23 amino groups and possible distortions of the folded state required to accommodate the disulfide bonds.

Depending on the position of insertion of a disulfide bond on the hydrophobic or polar surface of the melittin amphipathic helix, the cross-linked dimers conform to a well-defined structure or nondiscrete aggregates in solution. At high pH, or in the presence of divalent anions, $(mltK23C)_2$ adopts the form of a melittin-like pseudotetramer. A description of the solution association properties of these disulfide-dimerized melittins is important in understanding their effects on membranes since interactions with membranes involve equilibria between aqueous and membrane phases. The high stability of the self-associated $(mltK23C)_2$

pseudotetramer with respect to dissociation at high ionic strength, for example, suppresses membrane association, limiting the measurement of ion channel activity under these conditions (G. Boheim, J. Takei, A. Reményi, and C. E. Dempsey, unpublished). We have initiated studies on the membrane activities of these dimerized melittins which will be described elsewhere.

APPENDIX

Self-Association of (mltK23C)$_2$ in Solution. Preliminary analysis of titration data indicated that dimerization of (mltK23C)$_2$ resulting from amino group titration and from dianion-induced dimerization can be treated separately; that is, titration of an amino group (probably the N-terminal amino group; see the Discussion) induces self-association in the absence of dianions, and dianions promote dimerization under conditions where the N-terminal amino group retains its positive charge. pH-dependent self-association data were analyzed by the following treatment according to minimal schemes describing self-association resulting from amino group titration (Scheme 1) or dianion binding (Scheme 2).

(A) pH-Induced Self-Association. In Scheme 1, M^+, M, and D denote protonated, unprotonated and dimerized (mltK23C)$_2$, respectively. The concentration of unprotonated

Scheme 1

$$M^+ \rightleftharpoons M; \quad 2M \rightleftharpoons D$$

monomer is dependent on the pH, according to the Henderson−Hasselbalch equation:

$$[M] = \frac{[M_o]}{1 + 10^{(pK_a - pH)}} \tag{3}$$

where $[M_o]$ is the total monomer concentration and pK_a refers to the N-terminal amino group. If there is very little deprotonated monomer, M, at equilibrium (since it readily dimerizes), then

$$[M_o] = [P_o] - 2[D] \tag{4}$$

where $[P_o]$ is the total protein concentration in terms of monomers. When the fluorescence intensities are defined at the low- and high-pH extremes (where either monomer or dimer predominates) as I_M and I_D, respectively, the proportion of the protein in the dimeric form, α_D, is given by

$$\frac{I - I_D}{I_M - I_D} = \frac{[M_o]}{[P_o]} = 1 - \alpha_D \tag{5}$$

$$\alpha_D = \frac{2[D]}{[P_o]} \quad \text{or} \quad [D] = \frac{\alpha_D[P_o]}{2} \tag{6}$$

From eq 5

$$[M_o] = [P_o] - \alpha_D[P_o] = [P_o](1 - \alpha_D) \tag{7}$$

By combining eqs 3 and 7 to give an expression for [M] and from eq 6, the dissociation constant of the (mltK23C)$_2$ dimer, K_D, can be written as

$$K_D = \frac{[M]^2}{[D]} = \frac{2[P_o](1 - \alpha_D)^2}{\alpha_D[1 + 10^{(pK_a - pH)}]^2}$$

which yields a quadratic form for α_D

$$\alpha_D{}^2 - \left\{2 + \frac{[1 + 10^{(pK_a - pH)}]^2 K_D}{2[P_o]}\right\}\alpha_D + 1 = 0 \tag{8}$$

The experimentally determined value of α_D can be fitted to the solution of eq 8 using an independently determined measure of K_D to give pK_a.

(B) Ligand-Induced Self-Association. For the ligand-induced self-association, the following scheme is considered, involving M (monomer), D (dimer), and L (divalent anion ligand) (such as succinate).

Scheme 2

$$2M \rightleftharpoons D; \quad D + nL \rightleftharpoons DL_n$$

The dissociation constants are

$$K_D = \frac{[M]^2}{[D]} \quad K_L = \frac{[D][L]^n}{[DL_n]} \tag{9}$$

Fluorescence intensities, the total protein concentration $[P_o]$, and the fraction of material in dimeric form are related in a similar manner to that described in eqs 5 and 6, giving

$$\frac{I - I_{DL_n}}{I_M - I_{DL_n}} = \frac{[M]}{[P_o]} = 1 - \alpha_D \tag{10}$$

$$\alpha_D = \frac{2[DL_n]}{[P_o]} \tag{11}$$

where I is the measured fluorescence intensity, I_{DL_n} is the fully ligand-bound and dimerized state, and I_M is the monomeric state. From eqs 9 and 11

$$\alpha_D = \frac{2[P_o](1 - \alpha_D)^2[L]^n}{K_D K_L} \tag{12}$$

which yields a quadratic form for α_D

$$\alpha_D{}^2 - \left(2 + \frac{K_D K_L}{2P_o[L]^n}\right)\alpha_D + 1 = 0 \tag{13}$$

The experimentally obtained value of α_D can be fitted to the solution to eq 13, where the concentration of the divalent anion is given by

$$[L] = \frac{[L_o]}{10^{(pK_a - pH)} + 1} \tag{14}$$

where $[L_o]$ is the total buffer concentration and pK_a is that of the buffer.

Equilibrium Unfolding. The structural stabilities of monomeric and dimerized peptides, expressed as the extrapolated free energy in water, ΔG_w, were obtained from intrinsic (Trp19) fluorescence intensities at different urea concentrations, according to the analysis of Staniforth et al. (*32*). The free energy of folding at a given denaturant concentration, ΔG_d, is given by the following equations.

$$\Delta G_d = -RT \ln K_{obs} \tag{15}$$

K_{obs}, the experimentally derived folding equilibrium constant at given urea concentrations is given by

$$K_{obs} = \frac{c_p h(1-x)}{(c_p x)^h} \tag{16}$$

$$x = \frac{c_u}{c_p} = \frac{F - F_{min}}{F_{max} - F_{min}} \tag{17}$$

where c_p and c_u are concentrations of total and unfolded protein, respectively, h is the stoichiometric constant of the folding−unfolding equilibrium (see below), x is the fraction of unfolded species, and F, F_{min}, and F_{max} are the fluorescence intensities at a given denaturant concentration and of fully folded and fully unfolded states, respectively. At high pH and a high divalent anion concentration, the stoichiometric value h was 4 for melittin and 2 for $(mltK23C)_2$ as determined from analysis of NMR line widths and stopped flow fluorescence spectroscopy (see Results and Discussion). ΔG_d and ΔG_w are related by the solvation free energy of the hydrophobic amino acid residue (ΔG_s) and m (the average number of internal amino acid residues exposed to solution during the unfolding).

$$\Delta G_d = \Delta G_w + m\Delta G_s \tag{18}$$

ΔG_s values at given denaturant concentrations are obtained empirically.

$$\Delta G_s = \frac{\Delta G_{s,m} c_D}{K_{den} + c_D} \tag{19}$$

where c_D is the concentration of the denaturant (urea), $\Delta G_{s,m}$ is the maximum solvation free energy at infinite denaturant concentration, and K_{den} is "denaturant constant" which represents the concentration of denaturant required to achieve $\Delta G_{s,m}/2$. We used 1.115 kcal mol^{-1} and 14.90 M for $\Delta G_{s,m}$ and K_{den}, respectively, as values for average proteins (*32*). Experimental data are fitted to eq 18 to determine ΔG_w and m.

ACKNOWLEDGMENT

We are grateful to Dr. Graham Bloomberg for the excellent synthesis of the cysteine analogues of melittin.

REFERENCES

1. Schubert, D., Pappert, G., and Boss, K. (1985) *Biophys. J. 48*, 327−329.
2. Dempsey, C. E. (1990) *Biochim. Biophys. Acta 1031*, 143−161.
3. Dufourc, E. J., Faucon, J. F., Fourche, G., Dufourcq, J., Gulik-Krzywicki, T., and Le Maire, M. (1986) *FEBS Lett. 201*, 205−209.
4. Dempsey, C. E., and Watts, A. (1987) *Biochemistry 26*, 5803−5811.
5. Terwilliger, T. C., and Eisenberg, D. (1982) *J. Biol. Chem. 257*, 6016−6022.
6. Dempsey, C. E., Bazzo, R., Harvey, T. S., Syperek, I., Boheim, G., and Campbell, I. D. (1991) *FEBS Lett. 281*, 240−244.
7. Pawlak, M., Meseth, U., Dhanapal, B., Mutter, M., and Vogel, H. (1994) *Protein Sci. 3*, 1788−1805.
8. Iwamoto, T., Grove, A., Montal, M. O., Montal, M., and Tomich, J. M. (1994) *Int. J. Pept. Protein Res. 43*, 597−607.
9. You, S., Peng, S., Lien, L., Breed, J., Sansom, M. S., and Wooley, G. A. (1996) *Biochemistry 35*, 6225−6232.
10. Baleja, J. D., and Sykes, B. D. (1994) *Biochem. Cell Biol. 72*, 95−108.
11. Reiter, Y., Brinkmann, U., Lee, B., and Pastan, I. (1996) *Nat. Biotechnol. 14*, 1239.
12. Kumer, A., Ernst, R. R., and Wüthrich, K. (1981) *Biochem. Biophys. Res. Commun. 95*, 1−6.
13. Rance, M., Sørensen, O. W., Bodenhausen, G., Wagner, G., Ernst, R. R., and Wüthrich, K. (1983) *Biochem. Biophys. Res. Commun. 117*, 479−485.
14. Braunschweiler, L., and Ernst, R. (1983) *J. Magn. Reson. 79*, 352−356.
15. Morris, G. A., and Freeman, R. (1978) *J. Magn. Reson. 29*, 433−462.
16. Wüthrich, K. (1986) *NMR of Proteins and Nucleic Acids*, Wiley, New York.
17. Brünger, A. T. (1992) *X-PLOR Version 3.1−A System for X-ray Crystallography and NMR*, Yale University Press, New Haven, CT.
18. Ryckaert, J.-P., Ciccotti, G., and Berendsen, H. J. C. (1977) *J. Comput. Phys. 23*, 327−341.
19. Talbot, J. C., Dufourcq, J., De Bony, J., Faucon, J.-F., and Lussan, C. (1979) *FEBS Lett. 102*, 191−193.
20. Wagner, G., Pardi, A., and Wüthrich, K. (1983) *J. Am. Chem. Soc. 105*, 5948−5949.
21. Bundi, A., and Wüthrich, K. (1979) *Biopolymers 18*, 285−298.
22. Bazzo, R., Tappin, M. J., Pastore, A., Harvey, T. S., Carver, J. A., and Campbell, I. D. (1988) *Eur. J. Biochem. 173*, 139−146.
23. Dempsey, C. E. (1988) *Biochemistry 27*, 6893−6901.
24. Hagihara, Y., Oobatake, M., and Goto, Y. (1994) *Protein Sci. 3*, 1418−1429.
25. Quay, S. C., and Condie, C. C. (1983) *Biochemistry 22*, 695−700.
26. Zhu, L. Y., Kemple, M. D., Yuan, P., and Prendergast, F. G. (1995) *Biochemistry 34*, 13196−13202.
27. Zhou, N. E., Kay, C. M., and Hodges, R. S. (1993) *Biochemistry 32*, 3178−3187.
28. O'Donoghue, S. I., Junius, F. K., and King, G. F. (1993) *Protein Eng. 6*, 557−564.
29. Lemmon, M. A., Flanagan, J. M., Treutlein, H. R., Zhang, J., and Engelman, D. M. (1992) *Biochemistry 31*, 12719−12725.
30. Schwarz, G., and Beschiaschvili, G. (1988) *Biochemistry 27*, 7826−7831.
31. Wilcox, W., and Eisenberg, D. (1992) *Protein Sci. 1*, 641−653.
32. Staniforth, R. A., Burston, S. G., Smith, C. J., Jackson, G. S., Badcoe, I. G., Atkinson, T., Holbrook, J. J., and Clarke, A. R. (1993) *Biochemistry 32*, 3842−3851.

BI9729007